THE JOURNAL OF PHYSICAL CHEMISTRY C

Article

pubs.acs.org/JPCC

Structure and Defect Chemistry of Low- and High-Temperature Phases of $LiBH_4$

S. A. Shevlin,*[,†] C. Cazorla,[‡] and Z. X. Guo[†]

[†]Department of Chemistry, University College London, London WC1H 0AH, U.K.

[‡]Institut de Ciència de Materials de Barcelona (ICMAB-CSIC), Campus UAB, 08193 Bellaterra, Spain

ABSTRACT: Density functional theory simulations were performed to resolve the recent controversy regarding the crystal structure of the low-temperature and high-temperature phases of the hydrogen storage and Li ion electrolyte material $LiBH_4$. It is demonstrated that, independent of hybrid free exchange-correlation functional, the experimentally proposed orthorhombic *Pnma* structure is energetically the most favorable low-*T* structure while the experimentally proposed hexagonal $P6_3mc$ structure is the most favorable high-*T* structure. Furthermore, we discover a new monoclinic *C*2/*c* structure for the high-temperature phase which is competitive in stability with the $P6_3mc$ structure. Both high-temperature $P6_3mc$ and *C*2/*c* structures are stable against dehydrogenation and formation of Li vacancies. For all high-temperature structures, the formation energy of the Li Frenkel defect is low at 0.50−0.90 eV, with major implications for Li ion transport properties.

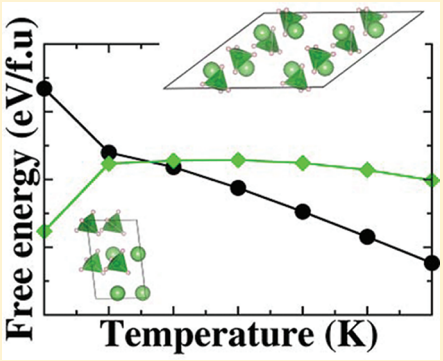

INTRODUCTION

There is a strong and pressing need to make a switchover to clean and efficient fuels in order to abate CO_2 emissions that cause undesirable climate change. In particular, hydrogen (H_2) is a favorable replacement as it has a high gravimetric energy density of 119 MJ/kg[1] and is easily obtainable from water (e.g., via thermolysis,[2] electrolysis,[3] or photocatalysis[4,5]). Typically, H_2 may be stored as a liquid at cryogenic temperatures (≤20 K), which involves the loss of approximately 30% of the energy density due to cooling requirements, or as a gas at room temperature and high pressures, necessitating the use of extremely strong and thick tank materials. However, the safe storage and utilization of hydrogen in these forms is technically difficult and costly, and therefore, solid-state condensed-phase materials that bind hydrogen in atomic form are preferred.[6] In particular, complex hydrides are promising materials for hydrogen storage applications as they have large gravimetric hydrogen storage capacities and are stable at room temperature.[7]

Lithium borohydride ($LiBH_4$) in particular is a promising material for hydrogen storage[7] and lithium superionic conduction applications.[8] At atmospheric pressure, solid $LiBH_4$ has two separate phases and undergoes a first-order transition from a low-temperature (LT) phase to a high-temperature (HT) phase at 381 K.[9] High Li ion mobility is only present in the high-temperature structure. Upon further heating, it is possible to liberate 13.1 wt % H_2 after melting at 560 K via a two-step reaction process

$$12LiBH_4 \rightarrow Li_2B_{12}H_{12} + 10LiH + 13H_2 \rightarrow 12LiH + 12B + 18H_2 \quad (1)$$

via the formation of an intermediate $Li_2B_{12}H_{12}$ phase.[10] By itself, however, $LiBH_4$ requires too high a temperature to desorb H_2; thus, research is ongoing in order to modify this material for applications.[11] It is therefore essential to know the crystal structure and quantify the binding of $LiBH_4$ before modification. However, the exact crystal structures of the low-*P*/low-*T* and low-*P*/high-*T* phases of $LiBH_4$ are contentious. In X-ray diffraction experiments (XRD), a phase transition from an orthorhombic unit cell with space group *Pnma* to a hexagonal unit cell with space group $P6_3mc$ was observed at 381 K.[12] Density functional theory (DFT) simulation accurately reproduces the structure of the LT phase;[13] however, it predicts the high-temperature hexagonal $P6_3mc$ phase to be vibrationally unstable.[14] Rather, DFT calculations find that a unit cell with space group *P*21/*c* is the likely ground-state HT structure,[15] although the hexagonal $P6_3mc$ unit cell has been reconfirmed with recent high-quality XRD experiments.[9] It has been suggested that the reasons for the disagreements between theory and experiment are related to the anharmonicity of low-frequency phonon modes associated with BH_4 rotation,[16] or significant disorder of hydrogen in the lattice.[17] On the basis of DFT-simulated annealing calculations, new candidate structures for both low-temperature and high-temperature phases have been proposed.[18] For the low-temperature phase, an orthorhombic unit cell of space group *Pnma* (with different lattice parameters compared to the experimental structure) was found to be thermodynamically favored. Furthermore, it was found that for the high-temperature phase a monoclinic unit cell of space group *P*2/*c* was lowest in energy. It is clear that there is

Received: February 14, 2012
Revised: May 15, 2012
Published: May 22, 2012

Table 1. Calculated Lattice Parameters (in Å) of the *Pnma* Low-Temperature Phases Using Different Functionals[a]

	SLT(*Pnma*)			TLT(*Pnma*)		
functional	*a*	*b*	*c*	*a*	*b*	*c*
PBE	7.274	4.371	6.521	8.484	4.348	5.750
PW91	7.274	4.371	6.521	8.484	4.348	5.750
LDA	6.869	4.189	6.298	8.339	4.175	5.113
PBESol	7.175	4.287	6.401	8.425	4.265	5.584
expt	7.179 (7.141)	4.437 (4.431)	6.803 (6.748)			

[a]Experimental lattice parameters at room temperature[12] (and in parentheses at 225 K[9]) are also shown.

still considerable debate regarding the crystal structure of $LiBH_4$.

In this paper, we perform first-principles DFT simulations on the crystal and thermodynamic properties of the experimental and theoretical (as proposed in ref 18) low-temperature and high-temperature crystal structures of $LiBH_4$. We demonstrate (via a calculation of the free energies as obtained within the quasi-harmonic approximation) that the new theoretical polymorphs suggested are thermodynamically less favorable than the structures obtained from experiment. In particular, we show that the experimental *Pnma* structure is energetically the most favorable low-temperature phase of $LiBH_4$ regardless of the exchange-correlation functional used. Furthermore, we demonstrate that the high-temperature phase of $LiBH_4$ proposed by Tekin et al. is vibrationally unstable, and that this result is independent of functional. We also discover a potential structure for the high-temperature phase which is monoclinic with space group $C2/c$ and show that it is competitive in stability terms with the experimentally proposed structure. Anharmonic effects on the enthalpy are determined and found not to be significant in modifying the differences in enthalpies (at room temperature) between different proposed high-temperature structures. In addition, for the first time the defect energetics of the high-temperature structure (of interest for both H-storage and Li-storage applications) are determined, and we demonstrate that the experimentally proposed structure has the largest defect formation energies while the structure proposed by Tekin et al. is the easiest to defect. Lithium ion Frenkel defects in particular are shown to possess interesting thermodynamics, with implications for superionic conduction applications.

COMPUTATIONAL METHODS

The VASP density functional theory code was used to calculate the structure and thermodynamics of the low-temperature orthorhomic *Pnma* phases proposed by Tekin et al. (denoted TLT(*Pnma*)) and Soulié et al. (denoted SLT(*Pnma*)) as well as the high-temperature $P2/c$ (denoted THT($P2/c$)) and $P6_3mc$ phases (denoted SHT(Cc)).[19] Density functional theory is a well-validated method for determining structures and energetics.[20] A plane-wave cutoff of 350 eV was used for geometry optimization and calculation of phonon spectra. In unit cell volume and lattice parameter optimizations, a higher plane wave cutoff of 450 eV was used in order to minimize possible Pulay stress bias and allow energies to be converged to less than 1 meV per formula unit. Calculations were performed using a variety of exchange correlation functionals, including PBE,[21] LDA,[22] PW91,[23] and PBESol.[24] However, unless otherwise discussed in the text, results are presented solely for the PBE functional. The projector augmented wave method was used to treat the core electrons, with the 1s electrons included.[25] The *k*-point mesh is sensitive to the structure. A Monkhorst–Pack net of $(4 \times 8 \times 8)$ was used for the LT phase unit cell calculations, while a Monkhorst–Pack net of $(3 \times 3 \times 3)$ *k*-points was used for the HT phase unit cell calculations. This *k*-point sampling produces converged energy differences for both phases, with errors less than 1 meV per formula unit. For calculations of native defects of the high-temperature structures, $2 \times 2 \times 2$ supercells were generated and a Monkhorst–Pack net of $(2 \times 2 \times 2)$ *k*-points was used. The total volume was not allowed to change during these calculations, but internal symmetry of the simulation cell is not constrained. All atoms were fully relaxed until the change in force upon ionic displacement was less than 0.01 eV/ Å.

The Helmholtz and Gibbs free energies of $LiBH_4$ for both theoretical and experimental *Pnma* phases were determined using essentially the same quasiharmonic approach as used by Tekin et al. and as we have used previously.[26,27] Our free-energy calculations were performed on a dense and wide grid of $V - T$ states in order to guarantee the condition that $P = 0$ over the whole temperature range $0 \leq T \leq 600$ K.

RESULTS

Low-*T* Phase. First, we compare the TLT(*Pnma*) and SLT(*Pnma*) crystals using four different types of exchange-correlation functional; see Table 1. The lattice parameters that we obtain for both structures using GGA functionals are very similar to those obtained in ref 18, and we would thus expect their thermodynamics to be extremely similar. As tends to be the case, we found that the LDA lattice parameters for both TLT(*Pnma*) and SLT(*Pnma*) structures are smaller than those found using GGA functionals, reflecting the tendency of the LDA to overbind. Among the family of GGA functionals we used, the PBESol functional finds the smallest lattice parameters, although they are still larger than those found with the LDA. Lattice parameters obtained from GGA functionals most closely match experiment. Crystal structures are shown in Figure 1. For the TLT(*Pnma*) structure the Li cation is tetrahedrally coordinated to the H atoms, specifically one tridentate H configuration and three bidentate H configurations. In contrast, for the SLT(*Pnma*) structure the Li cation is tetrahedrally coordinated to four bidentate H configurations. Regardless of the coordination of the Li ions, we find from a Bader analysis[28] that both TLT(*Pnma*) and SLT(*Pnma*) structures have extremely similar partial charges, with the Li cation having a charge of +0.89*e*, the B atom of the anion having a charge of +1.42*e*, and each atom of the H unit having a charge of −0.58*e*. As the partial charges are highly similar, we expect the nature of the binding between Li and BH_4 to be highly similar for the two phases. Our value for the charge transferred from cation to anion is in close agreement with the experimental value (+0.86*e*) found from synchrotron

dx.doi.org/10.1021/jp3014805 | J. Phys. Chem. C 2012, 116, 13488–13496

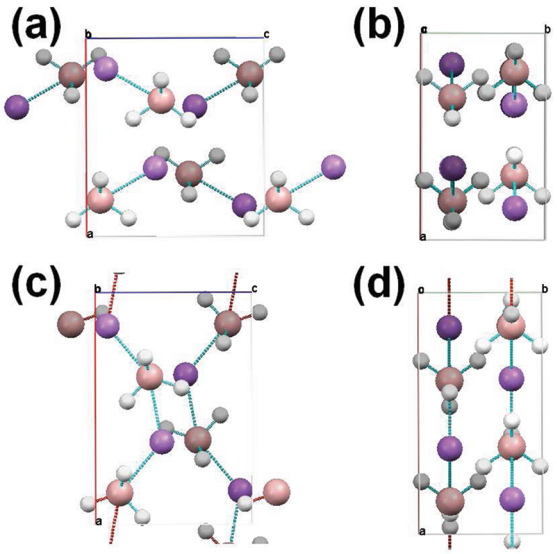

Figure 1. Crystal structure of the low-temperature phase of $LiBH_4$: (a,b) views of the SLT(*Pnma*) structure and (c,d) views of the TLT(*Pnma*) structure. Hydrogen atoms are represented by white spheres, boron pink, and lithium purple.

measurements, while we overestimate the charge transferred from B to H atoms in the covalently bound BH_4 unit, with experiment finding charges of +1.09*e* (B) and −0.49*e*(H).[29]

Similar Li−B, B−H, and Li−H distances are found for both SLT(*Pnma*) and TLT(*Pnma*) structures. This is reflected in the corresponding vibrational DOS (Figure 2) where the high-

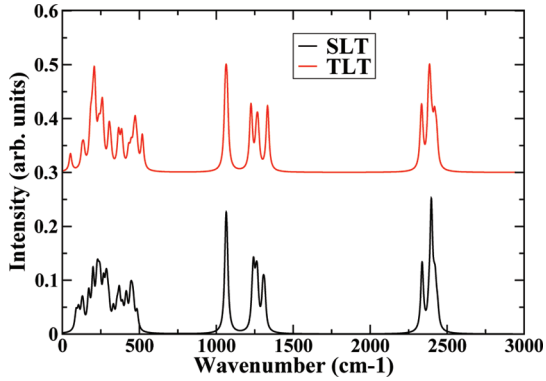

Figure 2. Vibrational DOS of TLT(*Pnma*) and SLT(*Pnma*) structures. The TLT(*Pnma*) spectrum has been arbitrarily shifted upward for comparison purposes.

frequency phonons represent B−H bond vibrations of the BH_4 tetrahedrons. Differences within the wavenumber interval $100 \leq \omega \leq 500$ cm^{-1}, corresponding to librational motion of the BH_4 tetrahedron,[30] are also observed. These differences manifest most significantly in the thermodynamics of the two phases as obtained from quasi-harmonic calculations. Without including temperature effects, we find that the SLT(*Pnma*) structure is lower in energy than the TLT(*Pnma*) structure (Table 2). The LDA functional predicts the strongest stability (in terms of energetics) for the SLT(*Pnma*) structure, while the GGA functionals all lessen the stability but still show that the SLT(*Pnma*) structure is the most stable. When including temperature effects as obtained within the quasi-harmonic approximation, the SLT(*Pnma*) structure still remains energeti-

Table 2. Calculated Energy Differences (Per Formula Unit) between SLT(*Pnma*) and TLT(*Pnma*) Structure[a]

functional	ΔE	ΔG
PBE	−0.005	−0.013
PW91	−0.002	−0.007
LDA	−0.006	−0.021
PBESol	−0.008	−0.009

[a] ΔE is electronic energy difference (E(SLT(*Pnma*)) − E(TLT(*Pnma*))), and ΔG is Gibbs free energy difference (G(SLT(*Pnma*)) − G(TLT(*Pnma*)) calculated at 300 K. Negative sign indicates SLT(*Pnma*) structure is preferred. All units are in eV.

cally the most favorable, as we show in Figure 3 where differences obtained with the PBE functional are plotted. As can

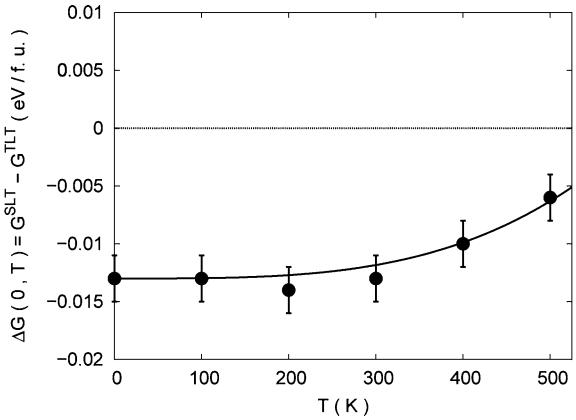

Figure 3. Ab initio equilibrium Gibbs free-energy difference between the experimentally determined[12] (exp) and theoretically predicted[18] (theo) *Pnma* low-*P*/low-*T* phases of $LiBH_4$, expressed as a function of temperature. Results were obtained within the quasiharmonic approximation using the small-displacement method.

be seen, including temperature further stabilizes the SLT(*Pnma*) structure over the TLT(*Pnma*) structure due to the effect of ionic entropy, which is crucial in determining the relative thermal stability of the polymorphs considered. Importantly, previous conclusions reached in the literature regarding the stability of structures were based on enthalpy calculations, which by definition do not include the effect of entropy. It is worth noting that we have found that the SLT(*Pnma*) structure is energetically the most favorable low-temperature phase of $LiBH_4$ and that this is the case regardless of the exchange-correlation energy functional used for comparing structures.

High-*T* Phase. *Crystal Structure.* The high-temperature structures (SHT(*Cc*) and THT(*P*2/*c*)) have also been investigated, with the crystal structures shown in Figure 4. Experimentally, the lattice parameters of the $P6_3mc$ structure are a = 4.276 Å and c = 6.948 Å, while simulation determined that the *P*2/*c* structure has lattice parameters a = 11.343 Å, b = 6.993 Å, and c = 8.780 Å.[18] First of all, we note that the THT(*P*2/*c*) structure possesses a strikingly large unit cell volume when compared to the corresponding low-*T* phase (either SLT(*Pnma*) or TLT(*Pnma*) structure). In particular, a hypothetical *T*-induced TLT(*Pnma*) → THT(*P*2/*c*) transformation, as reported in ref 18, would imply a $LiBH_4$ volume expansion of ∼110% per formula unit. This volume change is extraordinarily large and in complete disagreement with experiments where a volume contraction of 1.4% per formula

dx.doi.org/10.1021/jp3014805 | J. Phys. Chem. C 2012, 116, 13488−13496

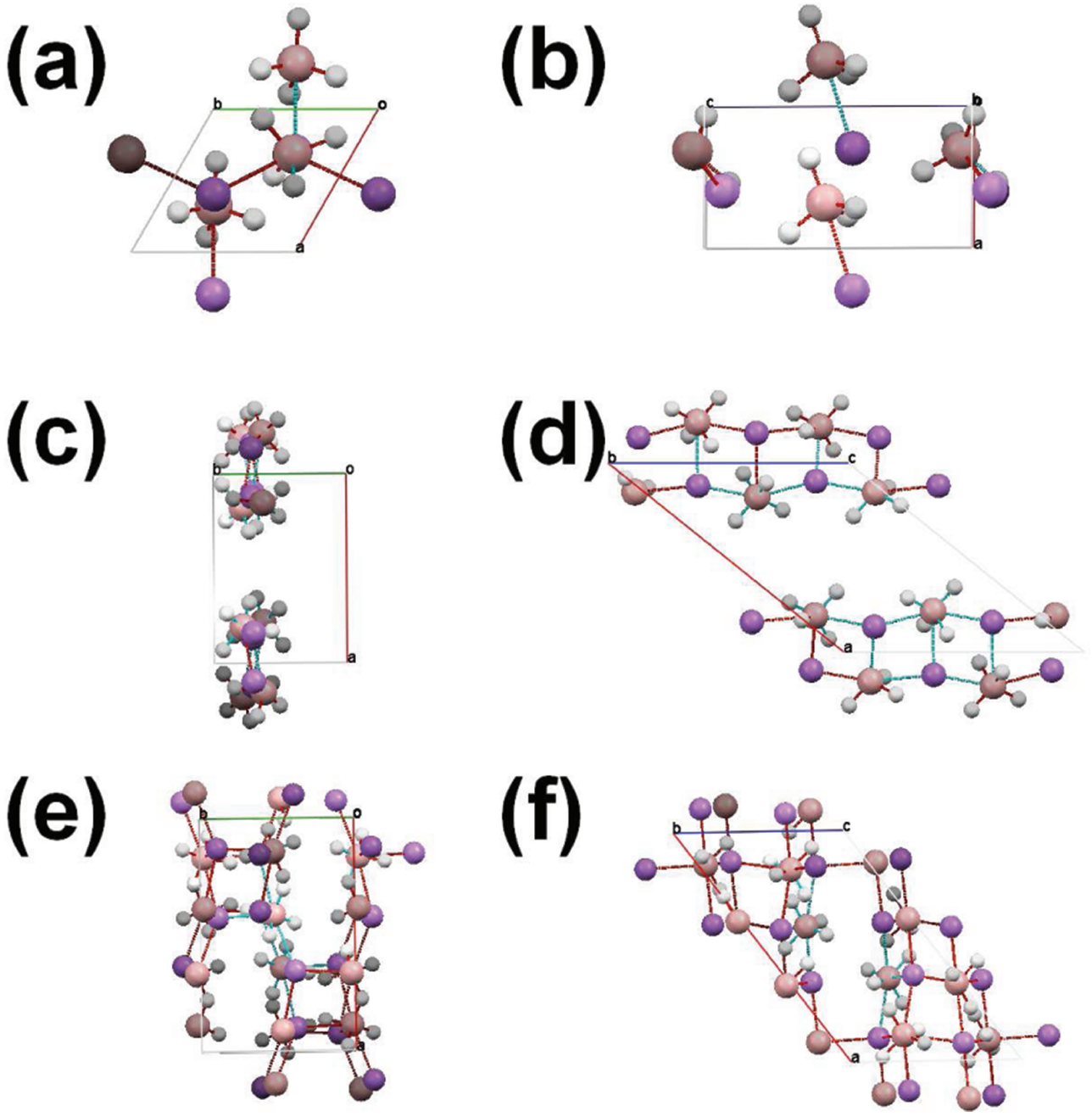

Figure 4. Crystal structure of the high-temperature phases of $LiBH_4$: (a,b) views of the SHT(Cc) structure; (c,d) views of the THT($P2/c$) structure; and (e,f) views of the SCHT($C2/c$) structure.

unit is observed.[9] From inspection it is evident that there are structural differences between the SHT(Cc) and THT($P2/c$) phases. In particular, the SHT(Cc) structure may be regarded as composed of linear Li−B−Li chains while the THT($P2/c$) structure may be regarded as composed of lines of alternating Li−B dimers. Additionally, in the SHT(Cc) structure the Li cation has one tridentate, two bidentate, and one monodentate coordination with H atoms of the BH_4 tetrahedra whereas for the THT($P2/c$) structure the Li cation has only three bidentate coordinations with H atoms of the BH_4 tetrahedra.

Upon relaxation (at zero temperature), a significant amount of reconstruction occurs for both structures. The SHT(Cc) phase reconstructs into a slightly distorted C_c structure with a slightly smaller volume (Table 3), gaining an energy of 0.058 eV per formula unit. The ideal C_c structure corresponds to that proposed by Łodziana et al.,[31] which is vibrationally stable at zero temperature. For the THT($P2/c$) structure we find that there is a significant reduction in volume, associated with an energy gain of 0.048 eV per formula unit. The volume reduction is due to a large contraction along the b-axis, which has the effect of reducing the vertical separation between $LiBH_4$ dimers. Nevertheless, the THT($P2/c$) structures that we obtain still have a greater volume than that of the low-temperature structures,which is in clear contradiction with experiment. Moreover, regardless of exchange-correlation functional used, all THT($P2/c$) structures are found to be vibrationally unstable, with one, or for the case of the LDA functional two, imaginary phonon modes. The frequencies of these imaginary modes in

dx.doi.org/10.1021/jp3014805 | J. Phys. Chem. C 2012, 116, 13488−13496

Table 3. Calculated Lattice Parameters (a, b, c in Å, and β) for the High-Temperature Phase of $LiBH_4$, after Relaxation Using Different Exchange Correlation Functionals[a]

phase	functional	a	b	c	β	volume
	PBE	4.124	7.359	6.629	98.4	49.75(0.96)
SHT(Cc)	PW91	4.124	7.359	6.629	98.4	49.75(0.96)
	LDA	4.017	6.876	6.240	85.6	42.96(0.95)
	PBESol	4.080	7.130	6.430	96.1	46.51(0.94)
	PBE	7.020	4.937	8.937	91.4	77.43(1.49)
THT($P2/c$)	PW91	7.072	5.011	8.942	91.2	79.38(1.53)
	LDA	6.042	4.034	8.489	94.6	51.57(1.14)
	PBESol	6.711	4.538	8.790	94.0	66.77(1.36)
	PBE	11.696	6.226	6.855	53.0	49.86(0.96)
SCHT($C2/c$)	PW91	11.687	6.236	6.841	53.2	49.92(0.96)
	LDA	9.534	4.898	6.794	67.6	36.67(0.81)
	PBESol	11.639	6.250	9.175	95.1	49.62(1.01)

[a]Top set is for the SHT(Cc) structure with space group Cc, middle set for the THT($P2/c$) structure with space group $P2/c$, and bottom set for the SCHT($C2/c$) structure with space group $C2/c$. Volume per formula unit for each unit cell in $Å^3$ is also given, with value in parentheses indicating relative change with respect to the volume per formula unit found for the SLT($Pnma$) phase (set to 1.0).

the long-wave limit are as follows: 46.3i (PBE), 39.4i (PW91), 65.6 and 74.1i (LDA), and 38.0i (PBESol). Previously, it has been found that stability of the SHT(Cc) structure is dependent on functional;[13] however, the fact that we find imaginary phonon modes in the THT($P2/c$) structure regardless of functional is highly indicative that this phase is unstable. Furthermore, this vibrational instability was present even when relaxation convergence criteria were tightened up significantly (to change in force upon ionic displacement was less than 0.001 eV/Å). Previous simulations found the THT($P2/c$) structure to be stable.[18] We attribute this difference to the fact that Tekin et al. used a different simulation code (CASTEP), norm-conserving pseudopotentials with a different number of valence electrons for the Li atom ($1s^2 2p_1$), and only use one type of functional.

Upon inspection of the THT($P2/c$) crystal structure obtained upon relaxation, we observed that there is a close similarity to crystals with the space group $C2/c$. We thus generated closely matching crystal structures as obtained using the ISOTROPY code.[32] Crystals with this space group generated immediately from the THT($P2/c$) structure were found to be vibrationally unstable within the PBE functional but stable with the other functionals. We thus further generated new crystal structures, by starting with orthorhombic modifications of the THT($P2/c$) structure (to match the space group of the LT structure) and then performed relaxations and space group analysis. As a result, we found stable $C2/c$ crystals with no imaginary phonons (regardless of functional). We denote this structure the SCHT($C2/c$) structure; see Figure 4 and Table 3. From inspection we oberve that the SCHT($C2/c$) structure has a dense network of Li–B bonds, differing from that of the SHT(Cc) and THT($P2/c$) structures. Each Li cation has three bidentate coordinations with H atoms of the BH_4 tetrahedra. The BH_4 tetrahedra are distorted, in agreement with the experimental results for the SLT($Pnma$) structure, although we observe B–H bond lengths vary from 0.93 to 1.23 Å. The SCHT($C2/c$) structure has a smaller volume per formula unit than the low-temperature phase, as observed by Soulié et al.[12] An important exception to this is the structure found with the PBESol functional, which has a volume per formula unit very slightly higher than the low-temperature phase. Temperature corrections to the lattice parameter might correct for this. Additionally, the XRD plots of the two candidate structures are quite similar for $2\theta \geq 10°$ (Figure 5), although there are considerably more peaks for the

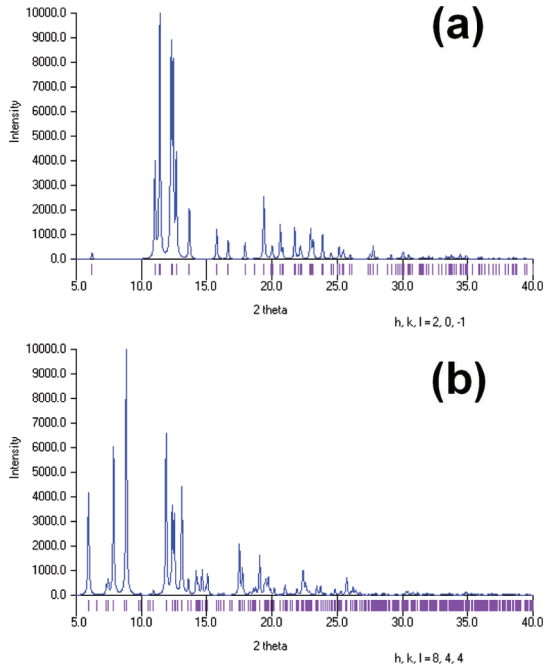

Figure 5. Calculated XRD patterns for the SHT(Cc) structure (a) and the SCHT($C2/c$) structure (b), where λ = 0.71 Å.

SCHT($C2/c$) structure below $2\theta \leq 10°$ allowing the possibility of experimental discrimination between the two structures. Broadening of the XRD peaks from thermal and nanocrystallite effects will further increase the similarity between SHT(Cc) and SCHT($C2/c$) XRD patterns for $2\theta \geq 10°$.

Thermodynamics. In order to determine the relative stability of the SHT(Cc) and SCHT($C2/c$) structures at zero and room temperature, we calculated the corresponding internal and Gibbs free energy differences (Table 4). Gibbs free energies were computed within the quasi-harmonic approximation for the crystal structures that were found to be vibrationally stable. Our zero-temperature results show that the THT($P2/c$) structure is higher in energy than the SHT(Cc) structure and that this structure is vibrationally unstable, thus

dx.doi.org/10.1021/jp3014805 | J. Phys. Chem. C 2012, 116, 13488–13496

Table 4. Calculated Electronic Energy Differences (ΔE) of the THT($P2/c$) and SCHT($C2/c$) Structures Compared to the SHT(Cc) Structure[a]

	THT($P2/c$)	SCHT($C2/c$)	
functional	ΔE	ΔE	ΔG
PBE	−0.071	0.021	−0.025
PW91	−0.076	0.021	−0.027
LDA	−0.212	0.009	−0.023
PBESol	−0.140	0.021	−0.003

[a]For the SCHT($C2/c$) structure the Gibbs free energy difference (ΔG) calculated at T = 300 K is also shown. Differences are per formula unit. Negative sign indicates SHT(Cc) structure preferred.

demonstrating that the THT($P2/c$) structure is unfavorable with respect to the SHT(Cc) structure for all temperatures below the melting point. In contrast, the SCHT($C2/c$) structure is actually favored over the SHT(Cc) structure at zero temperature. This may be due to the fact that the SCHT($C2/c$) structure has a larger unit cell with a lower symmetry, allowing it to manifest disorder effects that stabilize the cell.[9] Upon the inclusion of temperature effects the SHT(Cc) structure becomes the most stable regardless of the exchange-correlation functional used, although the stability as determined using PBESol is highly marginal at 0.003 eV/f.u. In order to illustrate this, we plot the Gibbs free energy differences between the low-T and prospective high-T structures, as calculated using both PBE functional and the PBESol functional (Figure 6). Here we see that for the PBE functional the

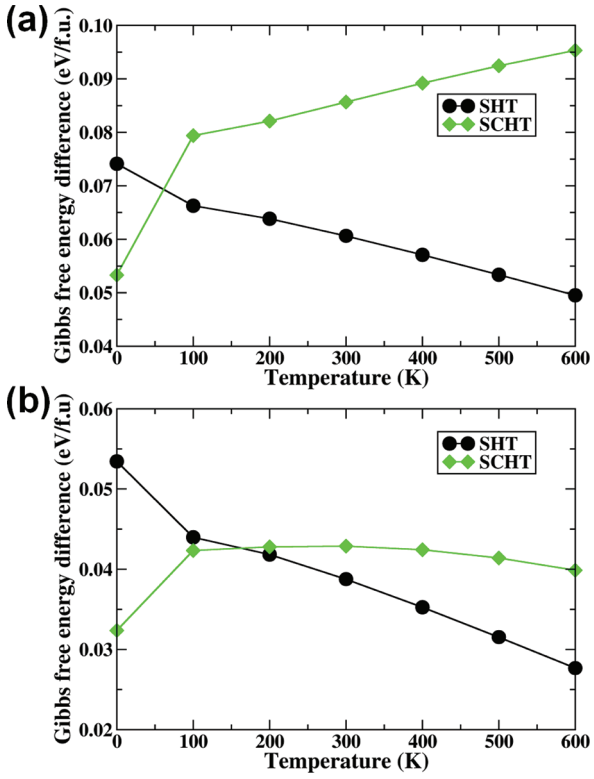

Figure 6. Gibbs free energy differences per formula unit for varying temperature for all vibrationally stable high-temperature structures with respect to the SLT($Pnma$) structure. Units are in eV. Top graph (a) shows results found using PBE, and bottom graph (b) shows results found using PBESol.

inclusion of temperature effects, even at low temperatures, has a strong effect upon the stability. Furthermore, only the SHT(Cc) structure shows a tendency with increasing temperature to become more stable with respect to the SLT($Pnma$) structure, with extrapolation indicating that crossover from the LT to the HT phase occurs at ∼1875 K, much larger than the experimental value of 385 K. The thermodynamics are different with the PBESol functional. Here, we see that as temperature increases both proposed high-temperature structures become more stable than the SLT($Pnma$) structure, as opposed to the PBE case where only the SHT(Cc) structure will become more stable. The SHT(Cc) structure will become more stable than the SLT($Pnma$) structure at ∼1160 K, while the SCHT($C2/c$) structure will become more stable at ∼1545 K. The SCHT($C2/c$) structure becomes the most energetically favored structure at ∼3385 K. These crossover temperature are highly sensitive to energy differences and thus errors in the exchange-correlation functional. The thermodynamics of the SCHT($C2/c$) structure strongly depend on functional, this can be understood in terms of phonon DOS. As for the low-temperature phase (Figure 2) the DOS of both SHT(Cc) and SCHT($C2/c$) structures splits into three branches. Within the quasi-harmonic approximation the lowest frequencies dominate the entropic effects. With the PBE functional we find that, normalizing the number of phonons to that per formula unit, the density of phonon frequencies in the low-frequency branch is higher in the SHT(Cc) than in the SCHT($C2/c$) structure (Figure 7).

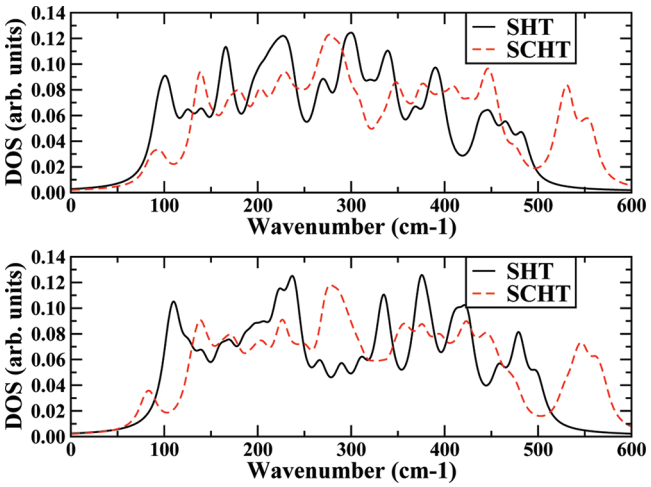

Figure 7. Phonon DOS of the high-temperature phase (SHT(Cc) and SCHT($C2/c$) structures). Only the low-frequency branch is shown, as this has the greatest impact on the thermodynamics. Top plot shows DOS calculated with the PBE functional, and bottom plot shows DOS calculated with the PBESol functional. All intensities are renormalized to allow easier comparison.

Therefore, as temperature increases entropic effects would tend to favor the SHT(Cc) structure, as shown in Figure 6. The opposite is true for the PBESol functional, where the lowest frequency phonon of the SCHT($C2/c$) structure is lower in frequency than that of the SHT(Cc) structure, and thus with increasing temperature entropic effects favor the SCHT($C2/c$) structure. This is related to the volume of the unit cell; although for the low-temperature phase PBESol structures have a smaller volume than PBE structures, this is not true for the high-temperature phase, where the PBESol unit cell has a greater volume than the PBE unit cell. Longer interatomic bonds result

dx.doi.org/10.1021/jp3014805 | J. Phys. Chem. C 2012, 116, 13488−13496

in lower frequency phonons, and thus a more stable SCHT($C2/c$) structure, thus explaining the functional-dependent behavior of the thermodynamics of the SCHT($C2/c$) structure. We also note in passing that the band gap of $LiBH_4$ is lower as obtained with the PBESol functional than that obtained with the PBE functional. It is clear then that at zero temperature and finite temperature the SCHT($C2/c$) structure is a viable contender for the high-temperature phase of $LiBH_4$. However, we emphasize that our calculations of temperature effects are performed within the quasiharmonic approximation, which may not be appropriate for high temperatures at which BH_4 tetrahedral rotation may occur.

We have attempted to estimate the effects of anharmonicity on the thermodynamics of the high-temperature structures by following the approach of Zarkevich et al.[16] In this we treat the different branches of the phonon DOS in different ways, namely, the high-frequency branches are treated purely within the quasiharmonic approximation, but the low-frequency branch is not. In particular, we assume that when including temperature effects the low-frequency phonons are purely anharmonic; i.e., rather than the kinetic and potential terms that apply to harmonic phonons, only kinetic terms apply. As each kinetic and potential degree of freedom may be regarded as contributing 1/2 kT to the enthalpy, it then follows that removing all potential terms equates to halving the temperature contribution of the phonon. Indeed, Zarkevich et al. have found from their molecular dynamics simulations of the high-temperature phase of $LiBH_4$ that when compared to the low-temperature phase three degrees of freedom stemming from potential energy terms are lost, and thus halving the temperature contribution of the low-frequency phonons. We use this approach to calculate the enthalpies of the SHT(Cc), SCHT($C2/c$), and THT($P2/c$) structures. Since calculation of the partition function of anharmonic phonons at heightened temperatures is nontrivial, we leave this for future work and restrict our discussion here to the enthalpies (Table 5). As above, two functionals are considered, PBE and PBESol. We observe that the SHT(Cc) structure is favored with the PBE functional, while the SCHT($C2/c$) structure is favored with the PBESol functional. Interestingly the PBE functional finds that the enthalpy differences between the SHT(Cc) and SCHT($C2/c$) structures are very small, in contrast to the Gibbs free energy differences obtained within the quasi-harmonic approximation which are significantly larger.

Table 5. Calculated Enthalpy Differences (Per Formula Unit) between the SHT(Cc) Structure and the SCHT($C2/c$) and THT($P2/c$) Structures, As Obtained at Two Temperatures Using Two Different Exchange Correlation Functionals[a]

enthalpy(temp, XC)	SCHT($C2/c$)	THT($P2/c$)
H(300,PBE)	−0.004	−0.071
H(600,PBE)	−0.006	−0.058
H(300,PBE)*	−0.007	−0.077
H(600,PBE)*	−0.008	−0.071
H(300,PBESol)	0.006	−0.136
H(600,PBESol)	0.001	−0.126
H(300,PBESol)*	0.015	−0.142
H(600,PBESol)*	0.013	−0.136

[a]Enthalpies marked with an asterisk include anharmonic effects. All units are in eV. Negative sign indicates that SHT(Cc) structure is preferred.

Trends in stability as temperature increases are qualitatively the same as for the Gibbs free energy. As can be seen in Table 5, including anharmonic effects to the enthalpy further stabilizes the SHT(Cc) over the SCHT($C2/c$) structure with the PBE functional, but destabilizes the SHT(Cc) structure over the SCHT($C2/c$) structure with the PBESol functional. This agrees with the data shown in Table 4, where the inclusion of entropy effects as shown in the Gibbs free energy has similar behavior. Therefore, since both anharmonic and entropy effects favor the stability of the same structure (SHT(Cc) with PBE, SCHT($C2/c$) with PBESol), quasi-harmonic Gibbs free energies provide qualitatively the correct stability results. Furthermore, we note that including anharmonic effects significantly increases the stability of the SCHT($C2/c$) structure within PBESol. The PBESol functional was developed to correct for the errors known to occur when using the PBE functional, and we are therefore inclined to believe that the PBESol results are more accurate. The difference in relative stabilities of the SHT(Cc) and SCHT($C2/c$) structures is purely due to the difference in the frequencies as calculated using the PBESol functional. These lower phonon frequencies correspond to a relative enthalpy difference of 1 meV at 300 K. This is due to the effect of the low-frequency phonon mode that occurs in this structure (Figure 7). Anharmonicity is more significant when comparing low-temperature and high-temperature structures.

Native Defects. Finally, in order to understand the defect properties of the high-temperature phase, of importance for hydrogen-storage and Li-electrolyte applications as defect chemistry is expected to strongly affect dehydrogenation and Li-transport mechanisms, we have determined the structure and defect formation energies (E_f) of several common defects. In particular, we have calculated the Li vacancy (V'_{Li}), BH_4 vacancy ($V^{\bullet}_{BH_4}$), Schottky defect ($V'_{Li} + V^{\bullet}_{BH_4}$), the lithium interstitial ($Li^{\bullet}_{i}$), and the lithium Frenkel defect ($V'_{Li} + Li^{\bullet}_{i}$), considering all of them as neutrally charged. Including charging will result in small negative corrections to our defect formation energies. Our results are shown in Table 6, as found using both PBE and PBESol functionals (which report similar values). Surprisingly, the Li Frenkel defect formation energy is the lowest for all structures considered. Furthermore, for the THT($P2/c$) structure the Li Frenkel defect formation is negative, again demonstrating that this structure is thermodynamically unstable with respect to Frenkel disorder. This implies that Li cation movement in this phase would strongly distort the structure, preventing further Li cation diffusion. This

Table 6. Calculated Defect Formation Energies for the High-Temperature Structures of $LiBH_4$[a]

	V'_{Li}	$V^{\bullet}_{BH_4}$	$Li^{\bullet}_{i}$	$V'_{Li} + V^{\bullet}_{BH_4}$	$V'_{Li} + Li^{\bullet}_{i}$
SHT(Cc)	4.20	3.89	1.37	3.40	0.50
SCHT($C2/c$)	4.31	3.84	1.82	3.57	0.90
SHT(Cc)	4.31	3.98	1.78	3.65	0.73
SCHT($C2/c$)	4.35	4.20	1.76	4.10	0.73

[a]Reference energies for Li atoms are taken to be those of the bulk, whereas for the BH_4 unit the reference energy is taken to be $BH_3 + {}^1/_2H_2$. Top two rows are for defects calculated with the PBE functional, and the bottom two for defects calculated with the PBESol functional. All units are in eV.

dx.doi.org/10.1021/jp3014805 | J. Phys. Chem. C 2012, 116, 13488−13496

is also in contrast with experimental results showing fast Li ion diffusion in the high-temperature phase. The SHT(Cc) and SCHT($C2/c$) structures have similar E_f, which further indicates that the SCHT($C2/c$) structure is a viable candidate structure for the high-temperature phase. Our calculated Li vacancy energies for the SHT(Cc) and SCHT($C2/c$) structures are of the same order of magnitude but higher than that reported by Du et al. who found a value for E_f of 3.77 eV.[33] However, we note that they modeled Li vacancy formation on the (010) surface of the low-temperature phase. Although it would be expected that the low-temperature phase would have higher Li ion vacancy formation energies, surface faceting would reduce the formation energy. Furthermore, the vacancy formation energies for the anionic BH_4 unit are smaller than the cation vacancy formation energies for the SHT(Cc) and SCHT($C2/c$) structures and thus are easier to replace. This agrees with experiments showing that it is possible to diffuse iodine into the high-temperature phase of $LiBH_4$ without changing the structure.[34] Upon defecting, neither the SHT(Cc) or SCHT-($C2/c$) structures show strong signs of reconstruction. Our calculated Li interstitial defect formation energies are considerably higher than the Li Frenkel energies, and it is unlikely that $LiBH_4$ is a good candidate Li ion electrode material. Our calculated Schottky defect energies are of the same order of magnitude (although slightly lower) as those found for Schottky defects in candidate Li ion electrode materials, e.g., $LiFeSO_4$ with a E_f of 4.22 eV.[35] However, our calculated Li Frenkel defect formation energies are significantly lower than those of candidate Li ion electrode materials, e.g. $LiFePO_4$ with a E_f of 2.15 eV,[36] or $LiFe_{0.50}Mn_{0.50}PO_4$ with a E_f of 2.75 eV.[37] This is highly intriguing because easy Li interstitial formation in the neutral crystal might be the mechanism behind the large Li ion conductivity of $LiBH_4$. In particular, Li ions in an interstitial site is a necessary precondition for Li ion transport, as the cations may easily migrate into an empty site under the influence of an electric field, as has recently being observed in ab initio nonequilibrium molecular dynamics.[38] However, we do not posit a direct relationship between defect energy and activation energy. Li ion transport will be investigated in a later work. Of the two stable high-T structures considered, the SHT(Cc) structure possesses the lower Li Frenkel defect formation energy. Calculation of defect formation energies provides further and definitive evidence that the THT($P2/c$) structure is not a viable structure for the high-temperature phase of $LiBH_4$.

CONCLUSIONS

We have demonstrated that, independent of hybrid free exchange-correlation functional and by considering entropy contributions to the free energy, the low-temperature (*Pnma*, denoted TLT(*Pnma*)) and high-temperature ($P2/c$, denoted THT($P2/c$)) structures proposed by simulation are not thermodynamically favorable with respect to the experimentally proposed structures. These thus may be excluded from the low-P region of the phase diagram of $LiBH_4$. Indeed, the THT($P2/c$) structure was found to be vibrationally unstable. Furthermore, we have discovered a new monoclinic stable structure for the high-temperature phase, with space group $C2/c$, which we denote SCHT($C2/c$), and is vibrationally stable regardless of the exchange-correlation functional used. This structure is energetically competitive with the experimentally proposed high-temperature structure and shows similar XRD diffraction patterns for large angle scattering ($2\theta \geq 10°$). Our discovery of this new prospective structure illustrates the complexity of the $LiBH_4$ phase diagram. The SCHT($C2/c$) structure would also be a candidate structure for high-pressure polymorphs of $LiBH_4$. Defect energetics of the high-temperature crystal phase were calculated, with the experimental structure having the greatest defect formation energies and the THT($P2/c$) structure having the lowest defect formation energies. For both stable high-temperature structures the Li cation vacancy has the largest formation energy. For all high-T structures the Li Frenkel defect is relatively easy to form, providing a rationale why the Li ion conductivity is so large for this material. The potential energy surface of $LiBH_4$ is quite complicated. Given the likely appearance of anharmonic effects at high T, all of the structures we have considered could be observed at thermodynamic conditions other than equilibrium and low T.

AUTHOR INFORMATION

Notes

The authors declare no competing financial interest.

ACKNOWLEDGMENTS

The authors acknowledge the use of the UCL *Legion* High Performance Computing Facility, and associated support services, in the completion of this work. The authors thank S.W.M. Myers for stimulating discussions. The authors acknowledge support by the EPSRC SUPERGEN Initiative under UK-SHEC (GR/S26965/01, EP/E040071/1), STEP-CAP (EP/G061785/1), and Platform Grant (GR/S52636/01, EP/E046193/1).

REFERENCES

(1) Züttel, A. *Naturwissenschaften* **2004**, *91*, 157.
(2) Kodama, T. *Prog. Energy Combust. Sci.* **2003**, *29*, 567.
(3) Greeley, J.; Jaramillo, T. F.; Bonde, J.; Chorkendorff, I. B.; Nørskov, J. K. *Nature Mater.* **2006**, *5*, 909.
(4) Catlow, C. R. A.; Guo, Z. X.; Miskufova, M.; Shevlin, S. A.; Smith, A. G. H.; Sokol, A. A.; Walsh, A.; Wilson, D. J.; Woodley, S. M. *Philos. Trans. R. Soc. A* **2010**, *368*, 3379.
(5) Shevlin, S. A.; Woodley, S. M. *J. Phys. Chem. C* **2010**, *114*, 17333.
(6) Lei, Y.; Shevlin, S. A.; Zhu, W.; Guo, Z. X. *Phys. Rev. B* **2008**, *77*, 134114.
(7) Orimo, S.-I.; Nakamori, Y.; Eliseo, J. R.; Züttel, A.; Jenson, C. M. *Chem. Rev.* **2007**, *107*, 411.
(8) Maekawa, H.; Matsuo, M.; Takamura, H.; Ando, M.; Noda, Y.; Karahashi, T.; Orimo, S.-I. *J. Am. Chem. Soc.* **2009**, *131*, 894.
(9) Fillinchuk, Y.; Chernyshov, D.; Černý, R. *J. Phys. Chem. C* **2008**, *112*, 10579.
(10) Ozolins, V.; Majzoub, E. H.; Wolverton, C. *J. Am. Chem. Soc.* **2009**, *131*, 230.
(11) Fang, Z. Z.; Kang, X. D.; Luo, J. H.; Wang, P.; Li, H. W.; Orimo, S.-I. *J. Phys. Chem. C* **2010**, *114*, 22736.
(12) Soulié, J. Ph.; Renaudin, G.; Černý, R.; Yvon, K. *J. Alloys Compd.* **2002**, *346*, 200.
(13) Shevlin, S. A.; Guo, Z. X. *Chem. Soc. Rev.* **2009**, *38*, 211.
(14) Miwa, K.; Ohba, N.; Towata, S.-I.; Nakamori, Y.; Orimo, S.-I. *Phys. Rev. B* **2004**, *69*, 245120.
(15) Frankcombe, T. J.; Kroes, G.-J.; Züttel, A. *Chem. Phys. Lett.* **2005**, *405*, 73.
(16) Zarkevich, N. A.; Johnson, D. D. *Phys. Rev. Lett.* **2008**, *100*, 040602.
(17) Dmitriev, V.; Filinchuk, Y.; Chernyshov, D.; Talyzin, A. V.; Ilewski, A.; Andersson, O.; Sundqvist, B.; Kurnosov, A. *Phys. Rev. B* **2008**, *77*, 174112.

(18) Tekin, A.; Caputo, R.; Züttel, A. *Phys. Rev. Lett.* **2010**, *104*, 215501.
(19) Kresse, G. *J. Comput. Mater. Sci.* **1996**, *6*, 15.
(20) Shevlin, S. A.; Fisher, A. J.; Hernández, E. *Phys. Rev. B* **2001**, *63*, 195306.
(21) Perdew, J. P.; Burke, K.; Ernzerhof, M. *Phys. Rev. Lett.* **1996**, *77*, 3865.
(22) Ceperley, D. M.; Alder, B. J. *Phys. Rev. Lett.* **1980**, *7*, 566.
(23) Perdew, J. P.; Chevary, J. A.; Vosko, S. H.; Jackson, K. A.; Pederson, M. R.; Singh, D. J.; Fiolhais, C. *Phys. Rev. B* **1992**, *46*, 6671.
(24) Perdew, J. P.; Ruzsinszky, A.; Csonka, G. I.; Vydrov, O. A.; Scuseria, G. E.; Constantin, L. A.; Zhou, X.; Burke, K. *Phys. Rev. Lett.* **2008**, *100*, 136406.
(25) Blöchl, P. *Phys. Rev. B* **1994**, *50*, 17953.
(26) Cazorla, C.; Errandonea, D.; Sola, E. *Phys. Rev. B* **2009**, *80*, 064105.
(27) Cazorla, C.; Alfè, D.; Gillan, M. J. *Phys. Rev. Lett.* **2008**, *101*, 049601.
(28) Sanville, E.; Kenny, S. D.; Smith, R.; Henkelman, G. *J. Comput. Chem.* **2007**, *28*, 899.
(29) Buchter, F.; Łodziana, Z.; Remhof, A.; Mauron, Ph.; Friedrichs, O.; Borgschulte, A.; Zuttel, A.; Filinchuk, Y.; Palatinus, L. *Phys. Rev. B* **2011**, *83*, 064107.
(30) Hagemann, H.; Gomes, S.; Renaudin, G.; Yvon, K. *J. Alloys Compd.* **2004**, *363*, 129.
(31) Łodziana, Z; Vegge, T. *Phys. Rev. Lett.* **2004**, *93*, 145501.
(32) Stokes, H. T.; Hatch, D. M.; Campbell, B. J. ISOTROPY, stokes.byu.edu/isotropy.html, 2007.
(33) Du, A. J.; Smith, S. C.; Yao, X. D.; Lu, G. Q. *J. Phys. Chem. C* **2007**, *111*, 12124.
(34) Borgschulte, A.; Gremaud, R.; Kato, S.; Stadie, N. P.; Remhof, A.; Züttel, A. *Appl. Phys. Lett.* **2010**, *97*, 031916.
(35) Tripathi, R.; Gardiner, G. R.; Islam, M. S.; Nazar, L. F. *Chem. Mater.* **2011**, *23*, 2278.
(36) Islam, M. S.; Driscoll, D. J.; Fisher, C. A. J.; Slater, P. R. *Chem. Mater.* **2005**, *17*, 5085.
(37) Gardiner, G. R.; Islam, M. S. *Chem. Mater.* **2010**, *22*, 1242.
(38) Aeberhard, P. C.; Williams, S. R.; Evans, D. J.; Refson, K.; David, W. I. F. *Phys. Rev. Lett.* **2012**, *108*, 095901.